LBL-37241
UC-413
Preprint

Lawrence Berkeley Laboratory
UNIVERSITY OF CALIFORNIA

Submitted to Nuclear Physics A

The Excitation of an Independent-Particle Gas—Classical or Quantal—by a Time-Dependent Potential Well

J. Blocki, J. Skalski, and W.J. Swiatecki

April 1995

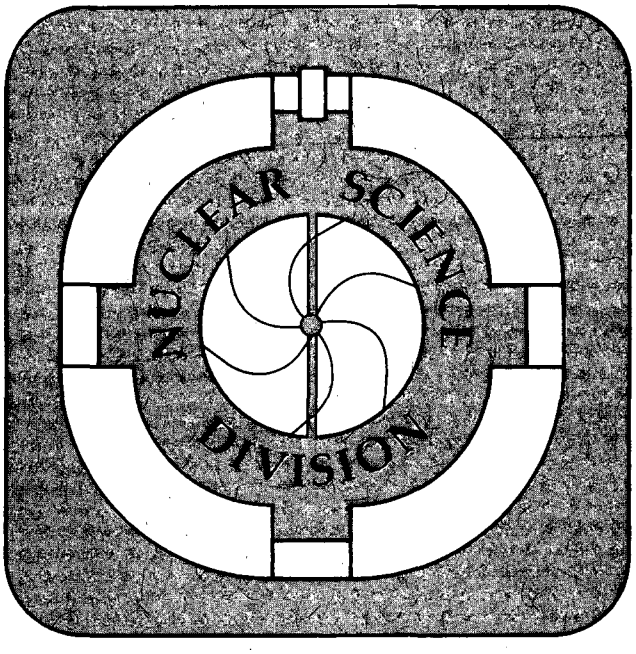

REFERENCE COPY
Does Not
Circulate
Bldg. 50 Library.
LBL-37241
Copy 1

Prepared for the U.S. Department of Energy under Contract Number DE-AC03-76SF00098

DISCLAIMER

This document was prepared as an account of work sponsored by the United States Government. While this document is believed to contain correct information, neither the United States Government nor any agency thereof, nor the Regents of the University of California, nor any of their employees, makes any warranty, express or implied, or assumes any legal responsibility for the accuracy, completeness, or usefulness of any information, apparatus, product, or process disclosed, or represents that its use would not infringe privately owned rights. Reference herein to any specific commercial product, process, or service by its trade name, trademark, manufacturer, or otherwise, does not necessarily constitute or imply its endorsement, recommendation, or favoring by the United States Government or any agency thereof, or the Regents of the University of California. The views and opinions of authors expressed herein do not necessarily state or reflect those of the United States Government or any agency thereof or the Regents of the University of California.

LBL-37241
UC-413

The Excitation of an Independent-Particle Gas—Classical or Quantal—by a Time-Dependent Potential Well

J. Blocki, J. Skalski, and W.J. Swiatecki

Nuclear Science Division
Lawrence Berkeley Laboratory
University of California
Berkeley, California 94720

April 1995

This work was supported by the Polish-American Maria Sklodowska-Curie Joint Fund II in cooperation with the National Science Foundation (U.S.) and the National Atomic Energy Agency (Poland), under project EMB ID# 70; and by the Director, Office of Energy Research, Division of Nuclear Physics of the Office of High Energy and Nuclear Physics, of the U.S. Department of Energy under Contract No. DE-AC03-76SF00098.

LBL-37241

The Excitation of an Independent-Particle Gas—Classical or Quantal—by a Time-Dependent Potential Well

J. Blocki,* J. Skalski,** and W.J. Swiatecki

Nuclear Science Division
Lawrence Berkeley Laboratory
University of California
Berkeley, CA 94720

April 1995

ABSTRACT

A systematic numerical investigation of the excitation of a classical or quantal gas of non-interacting particles in a time-dependent potential well is described. The excitation energy was followed in time for one oscillation around the sphere for six types of deformation: spheroidal shapes and Legendre polynomial ripples P_2, P_3, P_4, P_5, P_6, with relative RMS amplitudes of 0.2. Ten different speeds of deformation and eleven different values of the diffuseness of the potential well were studied, making altogether 660 quantal and 660 classical time-dependent calculations. In the upper range of deformation speeds the quantal results for the non-integrable shapes P_3–P_6 agree approximately with the wall formula for dissipation, the deviations being largely accounted for by the wave-mechanical suppression factor of S.E. Koonin et al., Ref. 4. For low deformation speeds the dissipation becomes dominated by one or two avoided level crossings.

1. INTRODUCTION

When it was realized that an independent-particle description of the atomic nucleus was, after all, a fair approximation, the model of a gas of non-interacting fermions in a more or less diffuse potential well (a "cavity" containing the gas) became the starting point of all theories of nuclear structure.

---

* Institute for Nuclear Studies, 05-400 Swierk, Poland.
**Institute for Nuclear Studies, Hoża 69, 00-681 Warsaw, Poland.

In dynamical processes such as nuclear fission or the fusion of two nuclei, the cavity in question changes its shape, usually at a rate small compared to the nucleonic speeds, and to a good approximation at fixed volume. Hence the following problem in theoretical dynamics presents itself: *To understand thoroughly the properties of a classical or quantal gas of independent particles in a slowly deforming cavity of fixed volume.*

The several decades since the introduction of the independent-particle model have seen considerable progress in the description of the dynamics of an idealized self-bound nuclear system (using, for example, the time-dependent Hartree-Fock method) including attempts to allow for such effects as the residual interactions between nucleons and the structural details of individual nuclei. Partly because a real nucleus *is* a considerably more complicated system than a gas of non-interacting point particles in an external potential, the dynamical problem posed in the preceding paragraph has not been investigated in a systematic way. Still, understanding even the drastically idealized problem of non-interacting particles in a time-dependent cavity should be helpful in understanding the true, complicated nuclear many-body problem, and a number of investigations have been devoted to this task. The principal result emerging from such studies points to the following situation: The response to slow shape changes of an independent-particle gas in a cavity depends dramatically on whether the particle motions are ordered (integrable) or chaotic. In the former case the gas responds as if it were an elastic solid, in the latter case a classical gas responds like a very viscous fluid, and a quantal gas responds similarly, except at *very* slow deformation speeds.

The above conclusions are based partly on theoretical considerations and partly on numerical computer simulations. The latter are relatively well documented in the case of classical particles, but are fragmentary for quantized particles. The present paper describes a systematic numerical study of quantal analogues of the corresponding classical calculations.

References 1–33 are a selection of currently available studies related to this problem, accompanied in some cases with attempts to compare the results with experimental data on nuclear fission and nucleus-nucleus collisions.

2. THE COMPUTER SIMULATIONS

The calculations reported in the present paper concern the excitation of a gas of quantal or classical particles in a container undergoing one cycle of an oscillation around the spherical shape. The container is either a sharp-walled cavity (square-well potential of infinite depth) or a diffuse cavity in the form of a Woods-Saxon potential well V(r,t) of finite depth V_0 and diffuseness a:

$$V(r,t) = -V_0 \Big/ \left[1 + \exp\left(\frac{r - R(t)}{a}\right)\right] . \tag{1}$$

(The sharp-walled cavity may be regarded as the limiting case when $a \to 0$, $V_0 \to \infty$.)

The cavities were taken to have axial symmetry and were described by a radius vector R(θ,t) given by

$$R = R(\theta,t) = \frac{R_0}{\lambda(t)}\left[1 + \alpha_n(t)P_n(\cos\theta) + \alpha_1(t)P_1(\cos\theta)\right] \tag{2}$$

for Legendre polynomial distortions, or by

$$\frac{R^2 \sin^2\theta}{b^2} + \frac{R^2\cos^2\theta}{c^2} = 1 \ , \tag{3}$$

where

$$c = R_0[1 + \alpha(t)] \ , \ b = R_0 \Big/ \sqrt{1 + \alpha(t)} \ , \tag{4}$$

for spheroidal deformations. In Eq. (2), $\alpha_n(t)$ was taken in the form

$$\alpha_n(t) = \sqrt{(2n+1)/5}\,\left(c_0 + c_1\cos\omega t\right) \quad , \quad n = 2,3,4,5,6 \tag{5}$$

and in Eq. (4)

$$\alpha(t) = c_0 + c_1\cos\omega t \ . \tag{6}$$

The factor $\sqrt{(2n+1)/5}$ ensures that the RMS deviation from the spherical shape is approximately the same for all six types of deformation. The normalizing factor λ(t) ensures volume conservation and the term $\alpha_1 P_1(\cos\theta)$ ensures fixity of the cavity's center of mass in the case of odd polynomial deformations P_3 and P_5. (Formulae for λ and α_1 may be found in Ref. 34.) In the cases reported in the present paper the mean deformation c_0 was always chosen to be zero,

and the amplitude c_1 was taken equal to 0.2. The oscillations thus start at t = 0 with the maximum (prolate) deformation, and they complete one cycle at $t = T = 2\pi/\omega$. In the case n = 2 the highest speed attained by a surface element occurs for $\theta = 0$ when $\omega t = \pi/2$, and is given by

$$v_{max} = c_1 \, \omega \, R_0 \quad . \tag{7}$$

We define the adiabaticity parameter η as the ratio of v_{max} to a nominal Fermi velocity v_F, of an N-fermion gas with a nominal Fermi energy T_F, i.e.,

$$\eta = \frac{c_1 \omega R_0}{v_F} \quad , \quad v_F = \frac{\hbar}{m R_0}\left(\frac{9\pi N}{4}\right)^{1/3} \quad , \quad T_F = \frac{\hbar^2}{2 m R_0^2}\left(\frac{9\pi N}{4}\right)^{2/3} \quad , \tag{8}$$

where m is the particle mass, taken as 938.928 MeV/c^2. Thus η is an approximate measure of the wall speed compared to the particle speeds. The cases studied correspond to ten values of η, equal to 0.02, 0.04, 0.06, 0.08, 0.10, 0.12, 0.24, 0.36, 0.48 and 0.60. The characteristic frequencies ω are thus related to η by

$$\hbar\omega = \frac{1}{c_1}\frac{\hbar^2}{m R_0^2}\left(\frac{9\pi N}{4}\right)^{1/3} \eta \approx 44.07 \, \eta \; MeV \quad , \tag{9}$$

with our choice of parameters. Thus, in the case of the quantal calculations, the cavity was filled at time t = 0 with 112 uncharged fermions, meant to represent the neutrons in a typical nucleus with mass number 184 and radius $R_0 = 1.16 \, A^{1/3} = 6.5978$ fm. Allowing for the axial symmetry of the potential and for the fermions' twofold degeneracy, there are typically 34 intrinsically different single-particle wave functions to be followed in time. The wave functions were evolved by a numerical solution of the Schrödinger equation (described in Appendix A). The relative total excitation energy of all the particles, given by

$$\Delta E / E_0 = [E(t) - E(0)]/E(0) \quad , \tag{10}$$

was then evaluated as a function of time.

In the case of the classical calculations, the cavity was filled with 20,000 particles whose initial positions and momenta were chosen at random to populate the phase space up to an energy

that would accommodate 112 particles at a phase-space density of 2 per h^3. The classical equations of motion were then followed as described in Appendix B.

3. RESULTS

Figure 1 is an overall summary of the results in the case of sharp-walled cavities, and gives the relative excitation energy at the end of one period as a function of the relative oscillation speed, as described by η. The six panels correspond to spheroidal, P_2, P_3, P_4, P_5, and P_6 deformations. The squares refer to classical and the circles to quantal calculations. The solid curves represent the classical wall formula, which at time t predicts a relative excitation energy given by

$$(\Delta E/E_0)_{WALL} = \tau + \tfrac{1}{5}\tau^2 \quad , \tag{11}$$

where

$$\tau = \tfrac{3}{4} c_1 \eta \left(\omega t - \tfrac{1}{2}\sin 2\,\omega t\right) \quad . \tag{12}$$

For $\omega t = 2\pi$ and $c_1 = 0.2$ this gives

$$(\Delta E/E_0)_{WALL} = 0.9425\,\eta + 0.1777\,\eta^2 \quad . \tag{13}$$

The dashed curves in Fig. 1 represent the result of using the following expression, derived in Ref. 4, which corrects the wall formula for the wave-mechanical suppression of the dissipation:

$$\frac{dE}{dt}\Big/\left(\frac{dE}{dt}\right)_{WALL} = 1 + \frac{x^2}{8} - \frac{x^2(8+x^2)}{16\left(2+\sqrt{4-x^2}\right)} + \frac{x^2}{8}\left(\frac{x^2}{4} - 4\right)\ln\left(2 + \sqrt{\frac{4-x^2}{x}}\right) \quad . \tag{14}$$

This suppression is associated with the finite ratio of the particle wavelengths to the wavelength of the multipole ripple of the oscillating cavity, given by x = (Fermi wavelength)/(Ripple wavelength). For a polynomial deformation of order n imposed on a sphere of radius R_0 the ripple wavelength is $2\pi R_0/n$. The Fermi wavelength for N fermions in the above sphere is

$$\lambda_F = 2\pi(4/9\pi N)^{1/3} R_0 \quad . \tag{15}$$

Thus

$$x = (4/9\pi N)^{1/3} n = 0.1081 n \quad for \quad N = 112 \quad . \tag{16}$$

The wave-mechanical suppression factors follow as 0.9571, 0.9110, 0.8510, 0.7785, 0.6946 for $n = 2, 3, 4, 5, 6$.

Figure 2 shows the time-history of the build-up of the excitations that result at $t = T$ in the circles in Fig. 1. The relative excitations are plotted in units of the wall formula's prediction for $t = T$, given by Eq. (13). The trend of the wall formula itself (the quotient of Eqs. (11) and (13)) is almost independent of η, and is shown by the dashed curve (drawn for $\eta = 0.24$).

Figure 3 shows the effect of diffuseness on the quantal excitations at $t = T$. The depth of the Woods-Saxon potential was taken as 200 MeV in order to minimize the escape of particles from the well. The label "diff" stands for the diffuseness parameter a in fm. Figure 4 is the analogous calculation for classical particles. Figures 5 and 6 show an attempt to estimate the effect of re-scaling the radius of the Woods-Saxon well so that the volume of the gas itself rather than of the half-depth potential contour would be the same for different values of the diffuseness.

4. DISCUSSION

The outstanding features of Fig. 1 are, first, that for not too small values of η (say $\eta \gtrsim 0.12$–0.24) the classical wall formula describes roughly the trend of the quantal calculations. Second, for these values of η, the quantal results are always below the wall formula but, in the case of the non-integrable deformations P_3, P_4, P_5, P_6, a good part of the deviation is accounted for by the wave-mechanical correction provided by Eq. (14). It is also remarkable that even in the case of integrable or near-integrable spheroidal and P_2 deformations the numerical results for large η approach the wall formula. In the classical case this is readily understood because in the short period of a sufficiently fast oscillation the particles do not have time to realize that they are moving in an integrable potential. It is comforting to know that this argument retains a measure of validity also for quantized particles. Figure 2 shows that for the higher η values the time dependence of the build-up of the excitation conforms qualitatively with the wall formula. For lower η values the results become more irregular. In the case of the spheroid the curves for $\eta = 0.04$ and 0.06 show the elastic (nearly reversible) behaviour familiar for particles in an

integrable potential. But the curve for $\eta = 0.02$ does not follow this trend. In the case of P_2 it is the curve for $\eta = 0.02$ that is most nearly reversible and $\eta = 0.04$ is not. In the case of P_3 and P_5 the curves for $\eta = 0.02$ and 0.04 exhibit wild swings, ending up at $t = T$ with more excitation than the wall formula prediction in the case of P_3, but less in the case of P_5. In the case of P_4 and P_6 the curves for $\eta \leq 0.12$ are considerably below the wall formula, sometimes by an order of magnitude.

A failure of the classical wall formula is indeed expected for very slow oscillations, for which the excitation will reflect the peculiarities of the time-dependent energy levels in the potential well. A detailed examination of the relevant level structures shows that the apparent irregularities referred to above correlate with the occurrence of avoided level crossings. At low deformation speeds a single avoided level crossing can dominate the excitation after one period of oscillation. However, since in the course of an oscillation cycle the avoided crossing is traversed twice (or possibly four times in the case of a reflection asymmetric shape) the application of repeated *asymptotic* Landau-Zener formulae that disregard phase relations between consecutive avoided crossings is quite inappropriate. On the contrary, interference effects can give rise to an oscillatory behavior of the excitation in its dependence on η. The oscillations are quite rapid, so that our calculations carried out at $\eta = 0.02, 0.04, 0.06, 0.08, 0.10, 0.12$ are not able to resolve them properly, and the results give the impression of an irregular behavior. Basing ourselves on a preliminary analysis, which included a semi-quantitative interpretation in terms of a simple two-level model along the lines of Ref. 35, we believe that these apparent irregularities can be understood in most cases in terms of relatively simple concepts. We hope to report on these studies at a later date.

Generally speaking, the wall formula will have a chance of approximating the quantal results if the typical level spacing is small compared to some energy characteristic of the oscillation speed, so that many levels will be taking part in the excitation process. From this point of view the present calculations do not correspond to situations where the wall formula would be expected to be at all accurate. Because of the assumed axial symmetry, the particles are divided

into separate groups labeled by the quantum number m, the projection of the angular momentum on the symmetry axis. In the case of reflection symmetric shapes, the parity π is also a conserved quantum number. The result is that, instead of a single gas with some 34 wave functions, one is dealing with several separate gases, each with, effectively, *only a few particles*. These gases do not communicate with one another during the deformation, and the level spacing for any one group is greater by an order of magnitude than what it would be in the absence of (m,π) conservation. This is illustrated in Fig. 7, which shows the energy levels in a sharp-walled cavity in the case of an $\alpha_4 P_4$ deformation with $\alpha_4 = 0.2\sqrt{9/5}$. The levels are grouped according to (m,π). There are altogether 12 non-communicating gases, five with one particle each, the most populous one having 7 particles and a typical level spacing of some 8 MeV. (Note that the value of η at which $\hbar\omega$, as given by Eq. (9), is equal to 8 MeV, is $\eta \approx 0.18$.) By contrast, if m and π were not good quantum numbers, the level spacing for 56 states containing 112 fermions would be about eight times smaller. The corresponding value of η beyond which a macroscopic wall formula would be useful might then be 0.01–0.03 in order of magnitude. In this connection note that for $\eta \leq 0.12$ the excitations for the P_3 and P_5 deformations are considerably closer to the wall formula than for P_4 and P_6 (Fig. 1). This is in line with the expectation that with parity conservation removed the relevant level density increases by a factor of two. But a more precise determination of the range of validity of the wall formula awaits a more exhaustive analysis and more extensive computer simulations.

In future studies aimed at establishing contact with the wall formula it would also be advisable to avoid oscillations around the spherical, integrable shape, for which the wall formula is not applicable.

Figures 3 and 4 illustrate the effect of increasing the diffuseness of the Woods-Saxon potential. In the quantal calculations this leads to a generally monotonic decrease of the dissipation. In the classical calculations the dissipation has a tendency to increase at first, before decreasing eventually to values comparable to (but generally higher) than the quantal dissipations. The interpretation of these results is made difficult by the fact that increasing the diffuse-

ness of a 200 MeV deep Woods-Saxon cavity containing 112 particles affects these particles in other ways besides making diffuse the cavity's wall. Because the particles fill only the lower one quarter of the potential well, an increase of the diffuseness at fixed mean volume of the Wood-Saxon potential decreases the *actual* effective volume in which the particles are confined, at the same time increasing the particles' Fermi energy and Fermi velocity, as well as introducing surface-layer corrections.

An attempt to estimate the change in dissipation due to this volume reduction of the gas was made along the following lines. Since, according to Eqs. (8) and (9), the relative excitation is inversely proportional to v_F and directly proportional to R_0, and since v_F and R_0 are both proportional to $\sqrt{T_F}$, the squeezing of the gas might be expected to reduce the value of $\Delta E/E_0$ by the factor $T_F(0)/T_F(a)$, where $T_F(a)$ is the Fermi energy of 112 particles in a potential with diffuseness a. In order to *undo* approximately the effect of the squeezing, we multiplied the values of $\Delta E/E_0$ in Figs. 3 and 4 by $T_F(a)/T_F(0)$. These factors range from 1.086 for $a = 0.1$ fm to 1.894 for $a = 1.0$ fm, as calculated in a Fermi gas approximation applied to a spherical Woods-Saxon potential. The results are shown in Figs. 5 and 6. The pronounced decrease of $\Delta E/E_0$ with increasing a has been largely removed, especially in the quantal results. Large irregularities remain in the case of P_3 (also P_5). The classical results usually show a maximum around $a = 0.3$–0.5 fm but, with some notable exceptions, the values of $\Delta E/E_0$ at $a = 1.0$ fm are generally comparable with the values at $a = 0$.

An alternative approach would be to remove the squeezing to begin with, by making R_o such an (increasing) function of a that the Fermi energy remained constant. We carried out a few such calculations for P_4 and P_6 with $\eta = 0.36, 0.48$. Qualitatively the effect was similar to that obtained by rescaling according to $T_F(a)/T_F(0)$. We hope to report in a future publication on a systematic study of the effects of surface diffuseness, together with a comparison with the theoretical expectations described in Ref. 7.

5. CONCLUSIONS

The present calculations represent a systematic study aimed at understanding the behavior of a quantal gas in a time-dependent cavity and its relation to corresponding classical results. The calculations explore the dependence of the energy dissipation on the speed of the deformation and on the multipolarity and diffuseness of the cavity. Even within the limitations of small particle numbers and large effective level spacings, one can discern a correspondence between the quantal excitations and the wall formula, especially after incorporating the wave-mechanical correction given by Eq. (14). However, because of the large effective level spacings, this correspondence emerges only for relatively large oscillation speeds ($\eta \gtrsim 0.12$–0.24). For lower values of η the excitation mechanism begins to be influenced by details of the level structures, being eventually dominated by a single avoided level crossing. Thus we have two regimes of deformation speeds: the *wall-formula regime* and the *avoided-crossing regime*. (See also Ref. 36.) One outstanding problem is the determination of the range of validity of the wall formula in situations more nearly approximating the fully chaotic case, where N fermions occupy N/2 different states in a potential that generates classical chaos. Our estimate is that the value of η characterizing the transition from a wall-formula behavior to an avoided-crossing behavior will be reduced by an order to magnitude in the case of such more nearly chaotic particle motions.

A second, longer-range objective, is to analyze further the avoided-crossing regime and, if possible, to incorporate the resulting insights in an approximate, usable equation of motion for the time-development of nuclear shape degrees of freedom. (In the wall-formula regime such a macroscopic equation of motion is discussed in Refs. 2 and 33.) The overall aim would be to achieve a macroscopic-microscopic method of handling nuclear dynamics, analogous to the corresponding method for describing nuclear static deformation energies.

ACKNOWLEDGMENTS

We would like to thank F. Brut, C. Jarzynski, and M. Wilkinson for discussions. J.B. and J.S. benefited from the hospitality of the Theory Group in the Nuclear Science Division at the

Lawrence Berkeley Laboratory on the occasion of several visits. W.J.S. would like to thank the organizers of the Mikolajki and Zakopane schools of physics for the opportunities that those meetings provided to continue the collaboration which resulted in the present paper.

This work was supported by the Polish-American Maria Sklodowska-Curie Joint Fund II in cooperation with the National Science Foundation (U.S.) and the National Atomic Energy Agency (Poland), under project EMB ID# 70; and by the Director, Office of Energy Research, Division of Nuclear Physics of the Office of High Energy and Nuclear Physics of the U.S. Department of Energy under Contract No. DE-AC03-76SF00098.

APPENDIX A: QUANTAL SOLUTIONS

Numerical solutions of the Schrödinger equation in a time-dependent cavity were obtained by expanding the wave functions in a suitable basis. In the case of the sharp-walled cavity the kinetic energy operator was first transformed to new coordinates, $\xi = r/R(\theta)$, θ, ϕ, where r, θ and ϕ are the usual spherical coordinates, and $R(\theta)$ is the radius vector specifying the axially symmetric cavity. In these new coordinates the cavity is spherical, but the kinetic energy operator no longer takes the form of the Laplace operator. Thus

$$\nabla^2 = \frac{\nabla^2_\xi}{R^2} + \frac{R^2_{,\theta}}{R^4}\left(\partial^2_\xi + \frac{2}{\xi}\partial_\xi\right) - \frac{R_{,\theta\theta} + ctg\theta\, R_{,\theta} + 2R_{,\theta}\partial_\theta}{R^3}\frac{1}{\xi}\partial_\xi \quad , \tag{A1}$$

where in the above formula ∇^2_ξ denotes the Laplace operator in the coordinates (ξ, θ, ϕ) and a comma denotes differentiation with respect to the suffix that follows.

In order to satisfy the boundary conditions we choose the basis to be a set of eigenfunctions of the spherical cavity in the ξ, θ, ϕ variables. Explicitly, these eigenfunctions are:

$$\phi_{m,l,n} = N_{l,n} j_l(a^l_n \xi)\, P^m_l(\theta) \frac{e^{im\phi}}{\sqrt{2\pi}} \quad , \tag{A2}$$

where j_l and a^l_n are the spherical Bessel functions and their roots, respectively, P^m_l are the associated Legendre polynomials with $l \geq m$, and $N_{l,n}$ are constant normalization factors.

The basis ϕ_μ, with $\mu = (nlm)$, depends on the deformation of the cavity $\alpha(t)$ as specified by Eqs. (1–6) in the text. The overlaps of the basis states, denoted by $\mathcal{N}_{\mu\nu}$, also depend on the deformation and are thus time-dependent in the course of the cavity's oscillation:

$$\mathcal{N}_{\mu\nu} = N_{l_1 n_1} N_{l_2 n_2} \int_0^1 \xi^2 j_{l_1}(a^{l_1}_{n_1}\xi) j_{l_2}(a^{l_2}_{n_2}\xi)\, d\xi \int_0^\pi \sin\theta\, P^m_{l_1}(\theta)\, P^m_{l_2}(\theta)\, R^3(\theta)\, d\theta \quad . \tag{A3}$$

The magnetic quantum number m is a constant of the motion, so the time-dependent Schrödinger equation can be solved separately in each subspace corresponding to a given m.

The matrix elements of the Hamiltonian contain three pieces corresponding to the three parts in Eq. (A1):

$$\mathcal{H}_{\mu\nu} = \frac{\hbar^2}{2M}\left(a_{n_2}^{l_2}\right)^2 N_{l_1 n_1} N_{l_2 n_2}\Big\{ I_{l_1 l_2}(a_{n_1}^{l_1}, a_{n_2}^{l_2}) \int_0^\pi \sin\theta\, P_{l_1}^m(\theta)\, P_{l_2}^m(\theta)\, R(\theta)\, d\theta$$
$$- J_{l_1 l_2}(a_{n_1}^{l_1}, a_{n_2}^{l_2}) \int_0^\pi \sin\theta\, P_{l_1}^m(\theta)\, P_{l_2}^m(\theta) \frac{R_{,\theta}^2}{R}\, d\theta \tag{A4}$$
$$+ K_{l_1 l_2}(a_{n_1}^{l_1}, a_{n_2}^{l_2}) \int_0^\pi \sin\theta \Big(P_{l_1}^m(\theta)\, \partial_\theta P_{l_2}^m(\theta) - \partial_\theta P_{l_1}^m(\theta)\, P_{l_2}^m(\theta) \Big) R_{,\theta} d\theta \Big\} \quad ,$$

where the quantities J and K can be expressed in terms of integrals over products of spherical Bessel functions as follows: let

$$I_{l_1 l_2}(a,b) = \int_0^1 \xi^2 j_{l_1}(a\xi) j_{l_2}(b\xi)\, d\xi \quad , \tag{A5}$$

where a and b are not necessarily the roots of j_{l_1} or j_{l_2}. Then

$$J_{l_1 l_2}(a_{n_1}^{l_1}, a_{n_2}^{l_2}) = \frac{l_2(l_2+1)}{(2l_2+1)(2l_2-1)} I_{l_1 l_2 - 2}(a_{n_1}^{l_1}, a_{n_2}^{l_2}) - \frac{2l_2^2 + 2l_2 - 3}{(2l_2+3)(2l_2-1)} I_{l_1 l_2}(a_{n_1}^{l_1}, a_{n_2}^{l_2})$$
$$+ \frac{l_2(l_2+1)}{(2l_2+1)(2l_2+3)} I_{l_1 l_2 + 2}(a_{n_1}^{l_1}, a_{n_2}^{l_2}) \quad , \tag{A6}$$

and

$$K_{l_1 l_2}(a_{n_1}^{l_1}, a_{n_2}^{l_2}) = \frac{l_2}{(2l_2+1)(2l_2-1)} I_{l_1 l_2 - 2}(a_{n_1}^{l_1}, a_{n_2}^{l_2}) + \frac{1}{(2l_2+3)(2l_2-1)} I_{l_1 l_2}(a_{n_1}^{l_1}, a_{n_2}^{l_2})$$
$$- \frac{l_2+1}{(2l_2+1)(2l_2+3)} I_{l_1 l_2 + 2}(a_{n_1}^{l_1}, a_{n_2}^{l_2}) \quad . \tag{A7}$$

The Schroedinger equation in the new coordinates reads

$$i\hbar\partial_t \psi = \left(\mathcal{H} + i\hbar\dot{\alpha} \frac{R_{,\alpha}}{R} \xi \partial_\xi \right) \psi \quad . \tag{A8}$$

A solution is expanded as:

$$\psi = \sum_\mu C_\mu(t)\, \phi_\mu \quad , \tag{A9}$$

and from Eq. (A8) we obtain a set of equations for the time-dependent expansion coefficients $C_\mu(t)$:

$$\sum_\nu \mathcal{N}_{\mu\nu} \dot{C}_\nu = \sum_\nu (\dot{\alpha} Z_{\mu\nu} - i\mathcal{H}_{\mu\nu})\, C_\nu \quad . \tag{A10}$$

Here, $\mathcal{N}$ is the overlap matrix, $\mathcal{H}$ is the instantaneous Hamiltonian matrix and $Z_{\mu\nu} = (\mu|\partial_\alpha \nu)$, given by

$$\mathcal{Z}_{\mu\nu} = N_{l_1 n_1} N_{l_2 n_2} \int_0^1 \xi^3 j_{l_1}(a_{n_1}^{l_1}\xi)\partial_\xi j_{l_2}(a_{n_2}^{l_2}\xi)\, d\xi \int_0^\pi \sin\theta\, P_{l_2}^m(\theta)\, P_{l_2}^m(\theta)\, R^2 R_{,\alpha} d\theta \quad . \qquad \text{(A11)}$$

The form of Eq. (A10), in which neither $\mathcal{Z}$ and $\mathcal{H}$ is hermitean, assures that the scalar product of any two state vectors is preserved under time evolution:

$$\frac{d}{dt}\left(\sum_{\mu\nu} \mathcal{N}_{\mu\nu} C_\mu^*(1) C_\nu(2)\right) = 0 \quad . \qquad \text{(A12)}$$

Each matrix element in the matrices in Eq. (A3), (A4) and (A11) can be expressed as a product, or as a sum of products, of two integrals: one, of the spherical Bessel functions, and the second, of the associated Legendre polynomials multiplied by a function of the cavity radius vector $R(\theta)$ and/or its derivative. The calculation of integrals involving Bessel functions can be performed once; integrals over the angle θ are deformation-dependent, and are performed repeatedly during the time-integration.

The calculation of the integrals over spherical Bessel functions were performed using the representation of the latter in terms of the Legendre polynomials. This results in a three-fold integral for $I_{l_1 l_2}(a,b)$, which is reduced to a two-fold integration over a natural interval [–1,1] of a product of Legendre polynomials with a simple function, which is a combination of exponentials and power functions. We used a double Gauss-Legendre integration scheme with 64 points. The results were checked with a direct integration over Bessel functions.

The integrals over θ were also performed using a Gauss-Legendre routine with 64 points. Only diagonal and next to diagonal matrix elements are calculated this way, the rest being generated using recurrence relations for associated Legendre polynomials.

The numerical integration of the time dependent Schrödinger equation, Eq. (A10), was carried out by means of the four-point predictor-corrector procedure. The initial four steps were performed using the second-order approximation to the exponential of the $\dot{\alpha}\mathcal{Z} - i\mathcal{H}$ operator.

The basis states included in the present calculations were those with $l \leq 32.5$, and $n \leq 9$, which restricts the energy of spherical states to less than $(32.5)^2$ in units of $\hbar^2/2mR_0^2$. In the same units, the Fermi energy of the system under consideration is around 100. As an example,

the dimension of the basis in the $m = 0$ subspace was 60 for positive parity, and 59 for negative parity states. As a check, calculations for several bases were repeated with an enlarged basis, with a cut-off energy corresponding to $a_n^l \leq 35.0$. The maximum angular momentum included was then $l = 28$, and the basis in the $m = 0$ subspace was enlarged to 76 and 69 states for positive and negative parity, respectively. The shift in static energies around the Fermi level was less than 0.1 MeV, and the differences in the relative excitation $\Delta E/E_0$ after one period of oscillation for the fastest deformation speed (corresponding to $\eta = 0.6$) were of the order of 0.001.

In the case of the diffuse cavity a more conventional expansion in a harmonic oscillator basis was used. To check convergence of the numerical results the number of oscillator shells was varied (up to 22) and the number of Gauss-Laguerre and Gauss-Hermite integration points used in evaluating the matrix elements was increased until a satisfactory accuracy was assured. The number of time steps required to get convergent results depended on the value of η. We found that for one period of oscillation an adequate number of time steps was 16000 for $\eta = 0.02$ and 800 for $\eta = 0.60$. To speed up the calculation the matrix elements of the Hamiltonian were not evaluated at each time step, but only after every 100 steps for $\eta = 0.02$ and after every 20 for $\eta = 0.60$, the intermediate matrix elements being calculated by linear interpolation. In the case of the P_4 oscillation and $\eta = 0.02$ the relative excitation was 0.062089, 0.059250 and 0.059105 when the number of points at which the matrix elements were actually evaluated was 40, 80 and 160, respectively.

An independent check of both versions of the quantal calculations is provided by their consistency. In Fig. 3 the values of $\Delta E/E_0$ calculated by the second program, when extrapolated to zero diffuseness, agree very nicely with the results of the first.

APPENDIX B. CLASSICAL SOLUTIONS

In the classical calculations the trajectory of a particle was followed by solving the classical equations of motion. In the case of the sharp-walled cavity, particles between bounces off the container walls move along straight lines. The numerical problem in this case is to find the point

in time and space of the collision of a particle with a moving wall. In the case of the diffuse Woods-Saxon potential the equation of motion must be integrated numerically all the way along the trajectory. This integration was performed by a four-point predictor-corrector method. The particles' initial conditions were chosen in a random Monte Carlo way assuming a uniform distribution in phase space, simulating a density $2/h^3$, where h is a Planck's constant. Thus the filling up of the potential with particles proceeded as follows. At each point in space the particle density is proportional to the third power of the local Fermi momentum, which is proportional to the square root of the depth of the potential with respect to the chemical potential (i.e., the Fermi energy). Integrating such a density and equating the result to the number of particles in the quantal case (N = 112) establishes the Fermi energy. This energy turned out to depend quite significantly on the diffuseness of the potential, being about 41 MeV for a Woods-Saxon diffuseness parameter $a = 0$ and about 77 MeV for $a = 1.0$ fm. This reflects the fact that the effective radius of the bottom part of the potential well decreases with increasing a. In order to get good statistics, 20000 trajectories were followed in each classical calculation.

Once again, an independent check of both versions of the classical computer program is provided by their consistency: in Fig. 4 the values of $\Delta E/E_0$ calculated for finite a extrapolate smoothly to the values at $a = 0$.

REFERENCES

1. D. Gross, Nucl. Phys. **A240** (1975) 472.
2. J. Blocki, Y. Boneh, J.R. Nix, J. Randrup, M. Robel, A.J. Sierk and W.J. Swiatecki, Ann. of Phys. **113** (1978) 338.
3. M.C. Robel, Independent Particle Aspects of Nuclear Dynamics, Ph.D. Thesis, Lawrence Berkeley Laboratory preprint LBL-8181 (1979), unpublished.
4. S.E. Koonin, R.L. Hatch and J. Randrup, Nucl. Phys. **A283** (1977) 87.
5. S.E. Koonin and J. Randrup, Nucl. Phys. **A289** (1977) 475.
6. J.R. Nix and A.J. Sierk, Phys. Rev. **C21** (1980) 982.
7. J. Randrup and W.J. Swiatecki, Ann. of Phys. **125** (1980) 193.
8. W.J. Swiatecki, Prog. Part. Nucl. Phys. **4** (1980) 383.
9. W.J. Swiatecki, Phys. Scripta **24** (1981) 113.
10. W.J. Swiatecki, Nucl. Phys. **A376** (1982) 275.
11. W.U. Schroeder and J. Huizenga in "Treatise on Heavy Ion Science," ed. D.A. Bromley, Plenum, 1983, Vol. 2, Chapter 3.
12. W.J. Swiatecki, Nucl. Phys. **A428**(1984) 199c.
13. J. Randrup and W.J. Swiatecki, Nucl. Phys. **A429** (1984) 105.
14. W.J. Swiatecki, in "Semiclassical Descriptions of Atomic and Nuclear Collisions" (North-Holland, 1985), p. 281.
15. J. Blocki, K. Grotowski, R. Planeta and W.J. Swiatecki, Nucl. Phys. **A445** (1985) 367.
16. N. Cârjan, A.J. Sierk and J. R. Nix, Nucl. Phys. **A452** (1986) 381.
17. W.Q. Shen, J. Albinski, A. Gobbi, S. Gralla, K.D. Hildebrand, N. Herrmann, J. Kuzminski, W.F.J. Mueller, H. Stelzer, J. Tōke, B.B. Brack, S. Bjørnholm and S.P. Sørensen, Phys. Rev. **C36** (1987) 115.
18. H. Feldmeier, Proc. 17th Mikolajki Summer School on Nuclear Physics, ed. Z. Wilhelmi, G. Skeflinska and M. Kicinska-Habior, Hardwood Academic Publishers 1987, p. 339.

19. W.J. Swiatecki, Nucl. Phys. **A488** (1988) 375c.

20. C.E. Aguiar, V.C. Barbosa, R. Donangelo and S.R. Souza, Nucl. Phys. **A491** (1989) 301.

21. W.J. Swiatecki, Proc. 21st Mikolajki Summer School on Nuclear Physics, ed. Z. Sujkowski and G. Szeflinska, Adam Hilger, Bristol, 1991, p. 219.

22. F. Brut, Proc. 21st Mikolajki Summer School on Nuclear Physics, ed. Z. Sujkowski and G. Szeflinska, Adam Hilger, Bristol, 1991, p. 235.

23. W.J. Swiatecki, Postepy fizyki **43** (1992) 507 (in Polish).

24. C. Jarzynski, Phys. Rev. **E48** (1993) 4340.

25. C. Jarzynski and W.J. Swiatecki, Nucl. Phys. **A552** (1993) 1.

26. J. Blocki, F. Brut and W.J. Swiatecki, Nucl. Phys. **A554** (1993) 107.

27. C. Jarzynski, Acta Physica Polonica **B24** (1993) 463.

28. J. Blocki, Y.-J. Shi and W.J. Swiatecki, Nucl. Phys. **A554** (1993) 387.

29. C.E. Aguiar, V.C. Barbosa, S.R. Souza and E.C. de Oliveira, Phys. Rev. **C47** (1993) 2396.

30. J. Blocki, F. Brut and W.J. Swiatecki, Acta Physica Polonica **25** (1994) 637.

31. J. Blocki, F. Brut, J. Skalski and W.J. Swiatecki, Fourth KINR International Conference on Nuclear Physics, Kiev, August 29–September 7, 1994, to appear in proceedings.

32. C. Jarzynski, Acta Physica Polonica **B25** (1994) 681.

33. W.J. Swiatecki, Nucl. Phys. **A574** (1994) 233c.

34. R.W. Hasse and W.D. Myers, "Geometrical Relationships of Macroscopic Nuclear Physics," Springer-Verlag, Berlin Heidelberg, 1988.

35. E. Shimshoni and Y. Gefen, Ann. of Phys. **210** (1991) 16.

36. M. Wilkinson and E. Austin, Phys. Rev. **A46** (1992) 64.

FIGURE CAPTIONS

Figure 1. The relative excitation $\Delta E/E_0$ of 112 formions in six types of cavities after one cycle of an oscillation around the spherical shape, plotted as a function of the speed of oscillation relative to the particle speeds (as given by the adiabaticity parameter η, defined by Eq. (8)). Squares refer to classical, circles to quantal computer simulations. The solid curves are the wall formula predictions, Eq. (13). The dashed curves incorporate the wave-mechanical correction according to Eq. (14).

Figure 2. The time-dependent relative excitations $\Delta E/E_0$ which, after one period, give the quantal excitations plotted as circles in Fig. 1. The labels specify the different deformation speeds as given by η.

Figure 3. The relative excitations $\Delta E/E_0$ after one period, plotted as functions of the diffuseness a of the Woods-Saxon potential, Eq. (1). The deformation speeds are identified by the symbols as follows: squares, $\eta = 0.06$; diamonds, $\eta = 0.12$; triangles, $\eta = 0.24$; circles, $\eta = 0.36$; asterisks, $\eta = 0.48$; stars, $\eta = 0.60$.

Figure 4. Same as Fig. 3 but for classical particles.

Figure 5. The values of $\Delta E/E_0$ in Fig. 3 were multiplied by a diffuseness-dependent factor designed to ensure approximate volume conservation of the actual particle distributions, rather than of the half-depth contour of the Woods-Saxon potential well.

Figure 6. This is like Fig. 5, but for the classical results.

Figure 7 The energy levels for a sharp-walled cavity with a $P_4(\cos\theta)$ deformation. The 112 particles occupy 34 states in 12 non-communicating groups, labeled by the angular momentum projection quantum number m and parity π, identified by + or – in the line above the m labels. The degeneracy is two for $m = 0$ and four for $|m| \neq 0$).

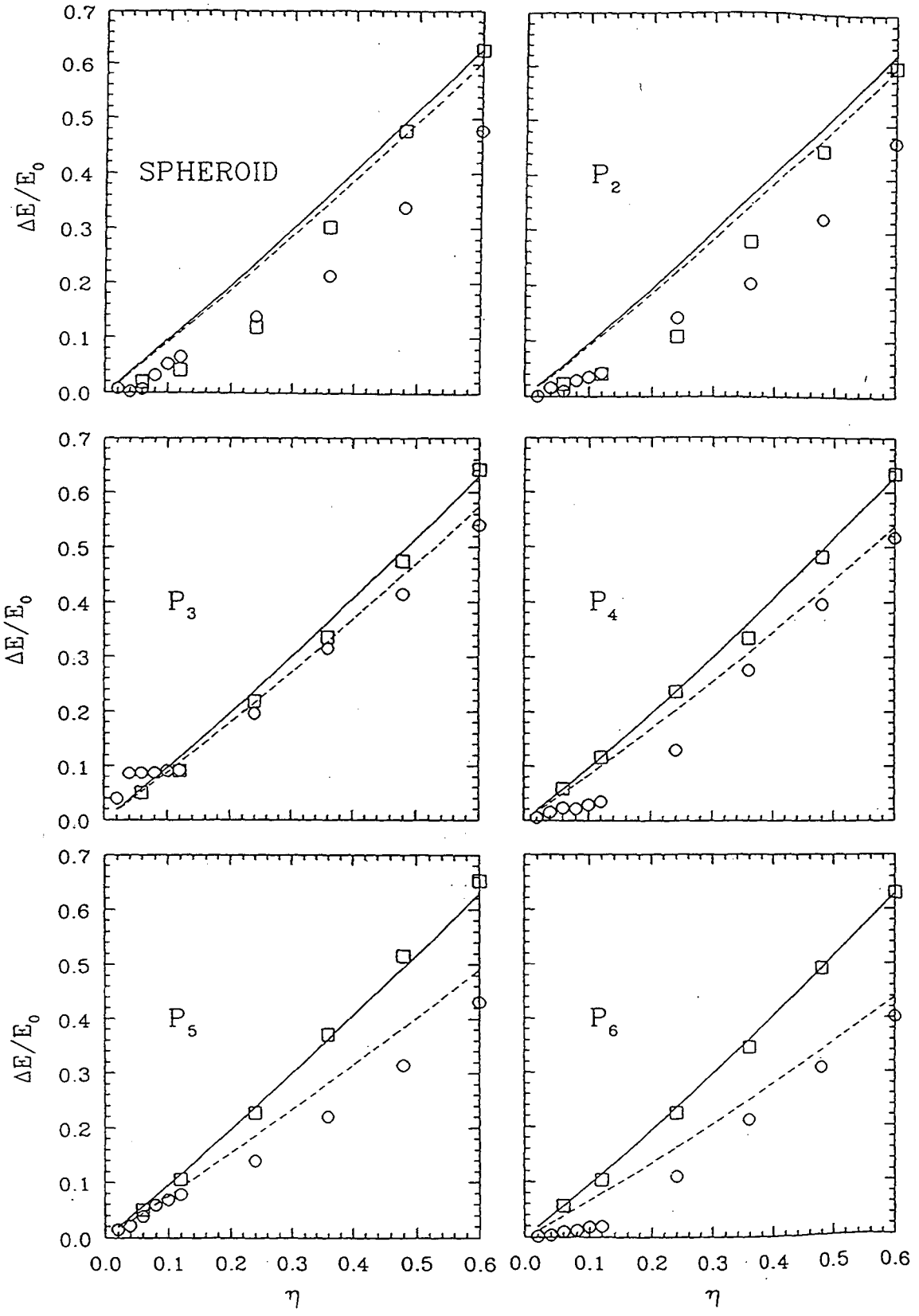
SPHEROID
P_2
P_3
P_4
P_5
P_6
$\Delta E/E_0$
η
0.0
0.1
0.2
0.3
0.4
0.5
0.6
0.7

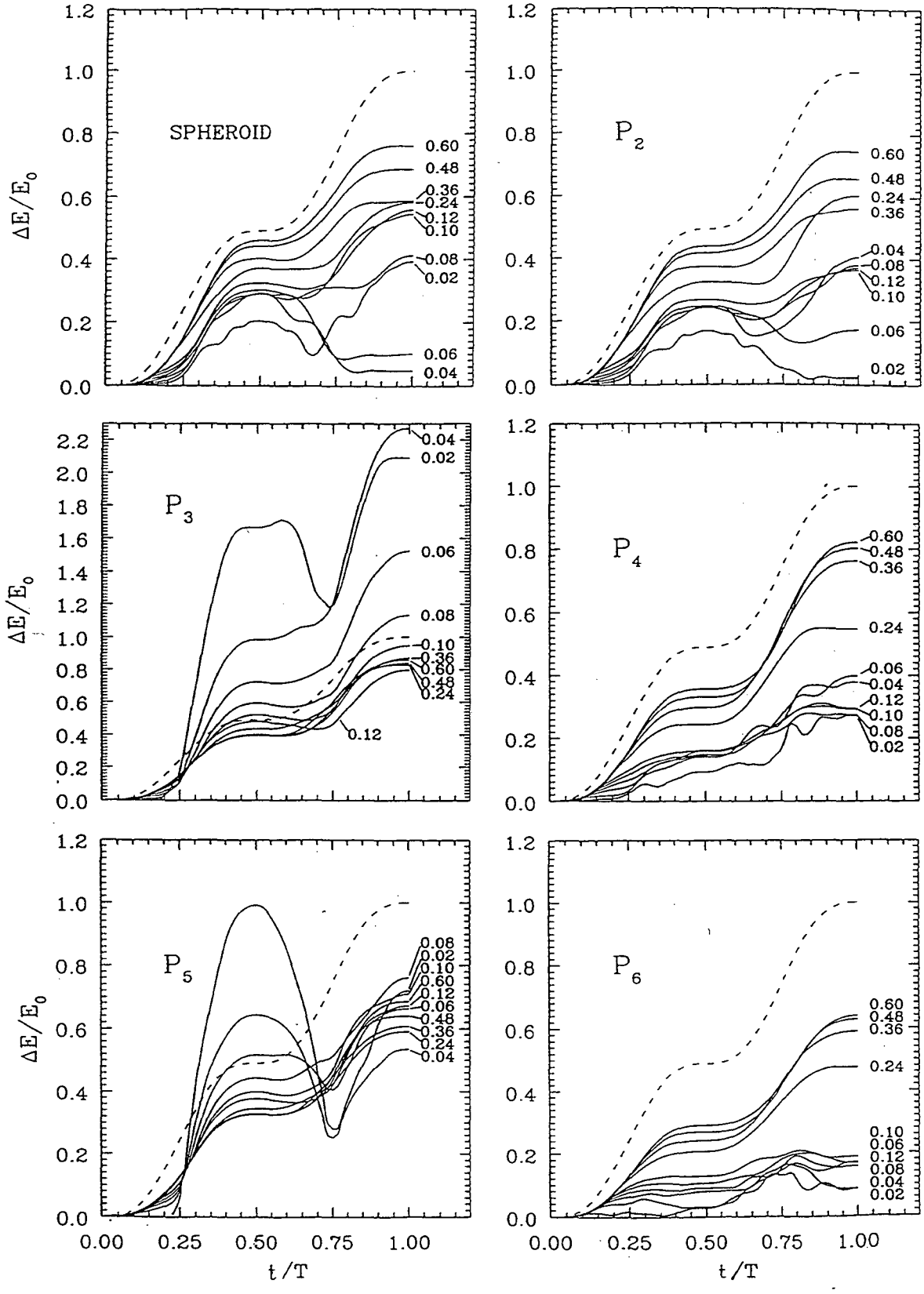
SPHEROID
P2
P3
P4
P5
P6
ΔE/E0
t/T
0.00
0.25
0.50
0.75
1.00
0.0
0.2
0.4
0.6
0.8
1.0
1.2
1.4
1.6
1.8
2.0
2.2
0.60
0.48
0.36
0.24
0.12
0.10
0.08
0.06
0.04
0.02

QUANTAL

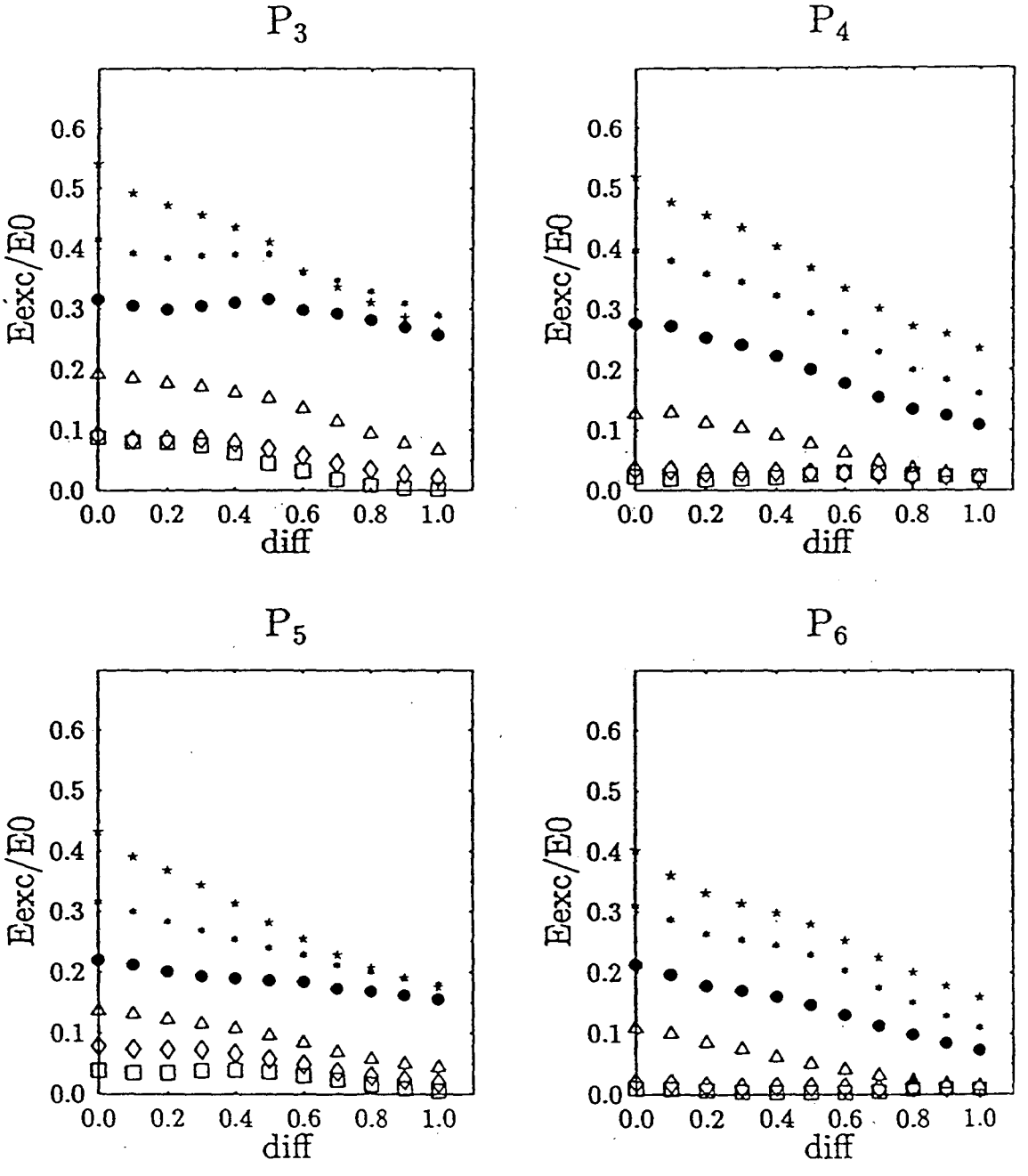

CLASSICAL

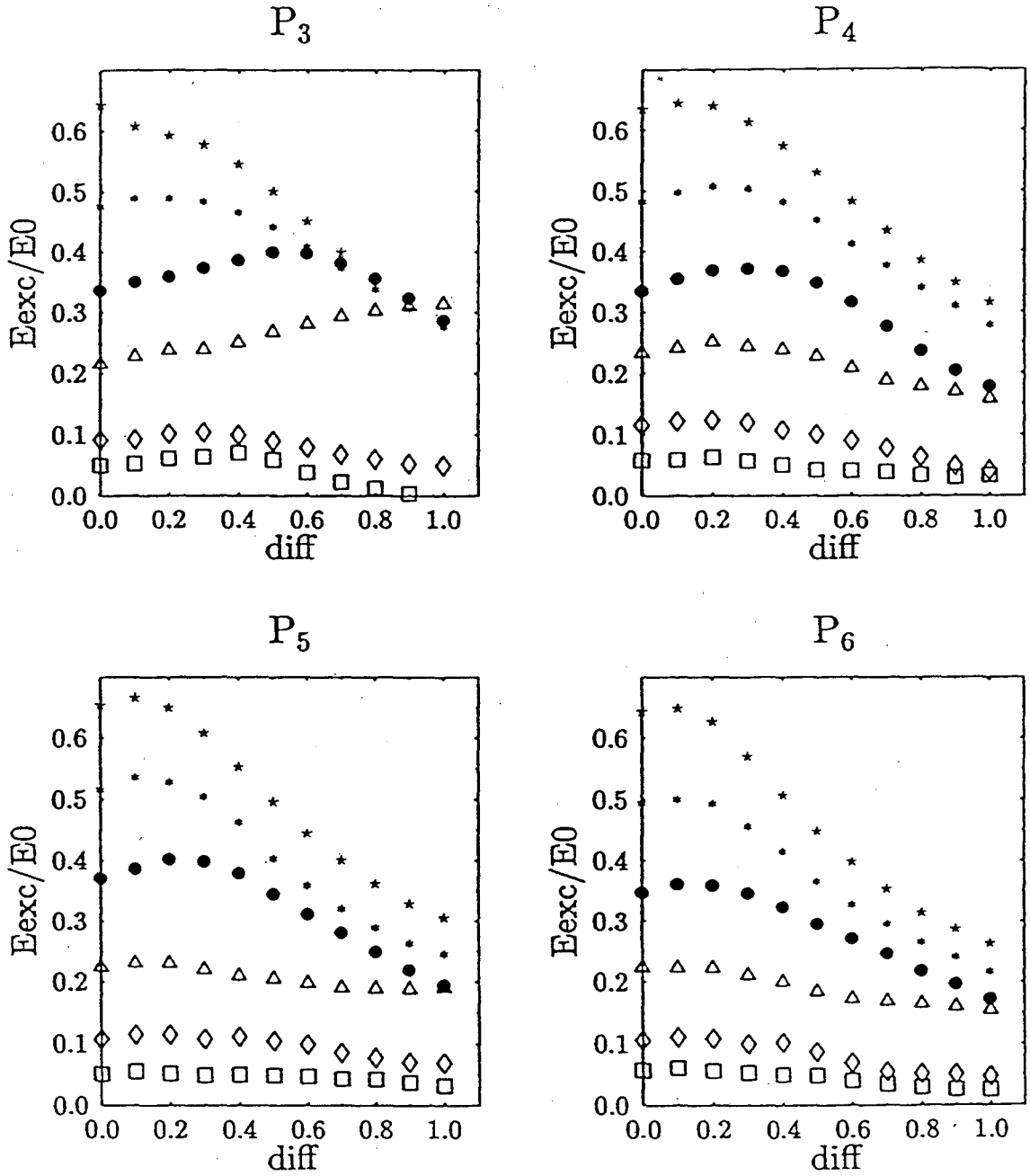

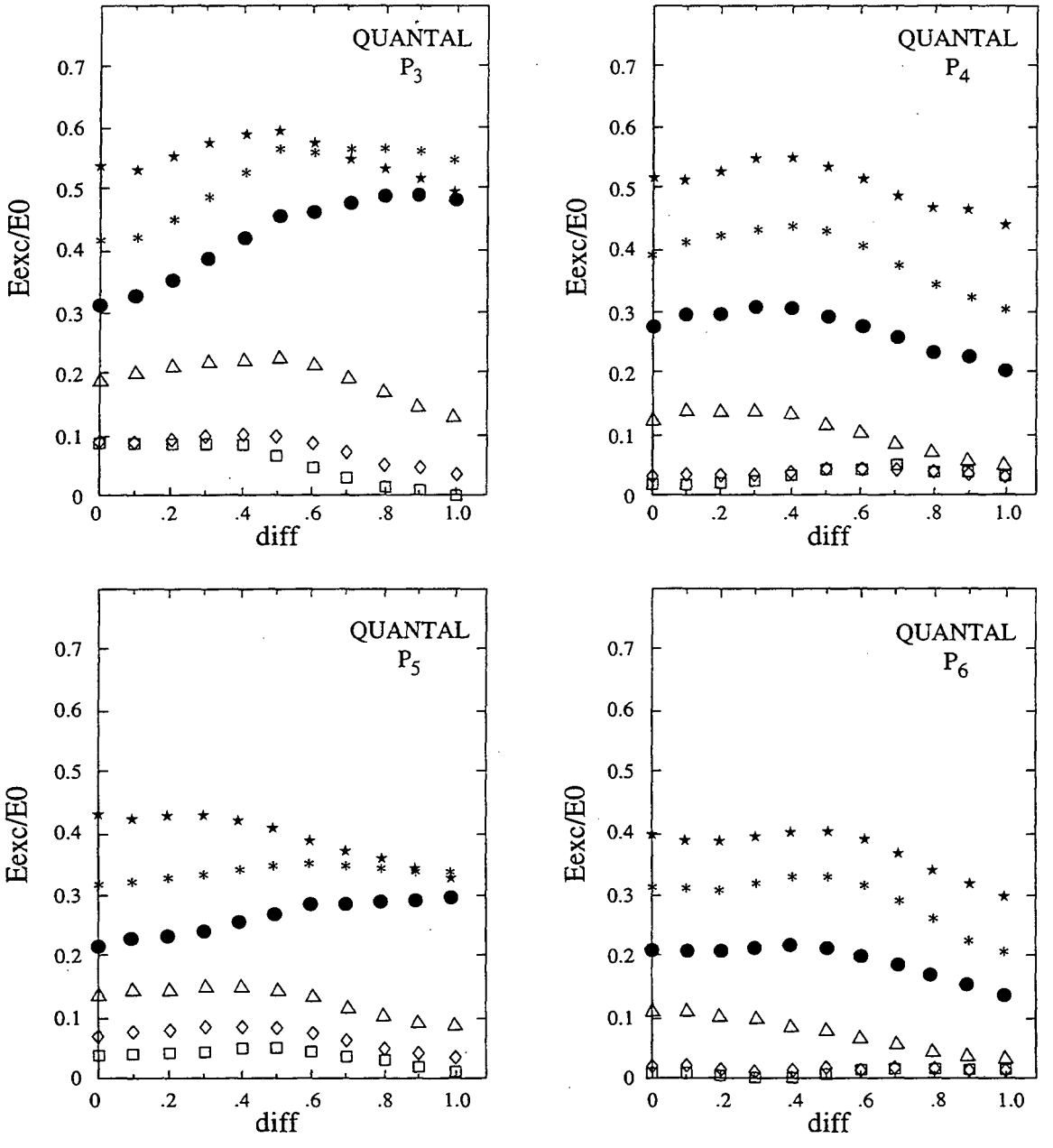
QUANTAL
P3
QUANTAL
P4
QUANTAL
P5
QUANTAL
P6
Eexc/E0
diff
0
0.1
0.2
0.3
0.4
0.5
0.6
0.7
.2
.4
.6
.8
1.0

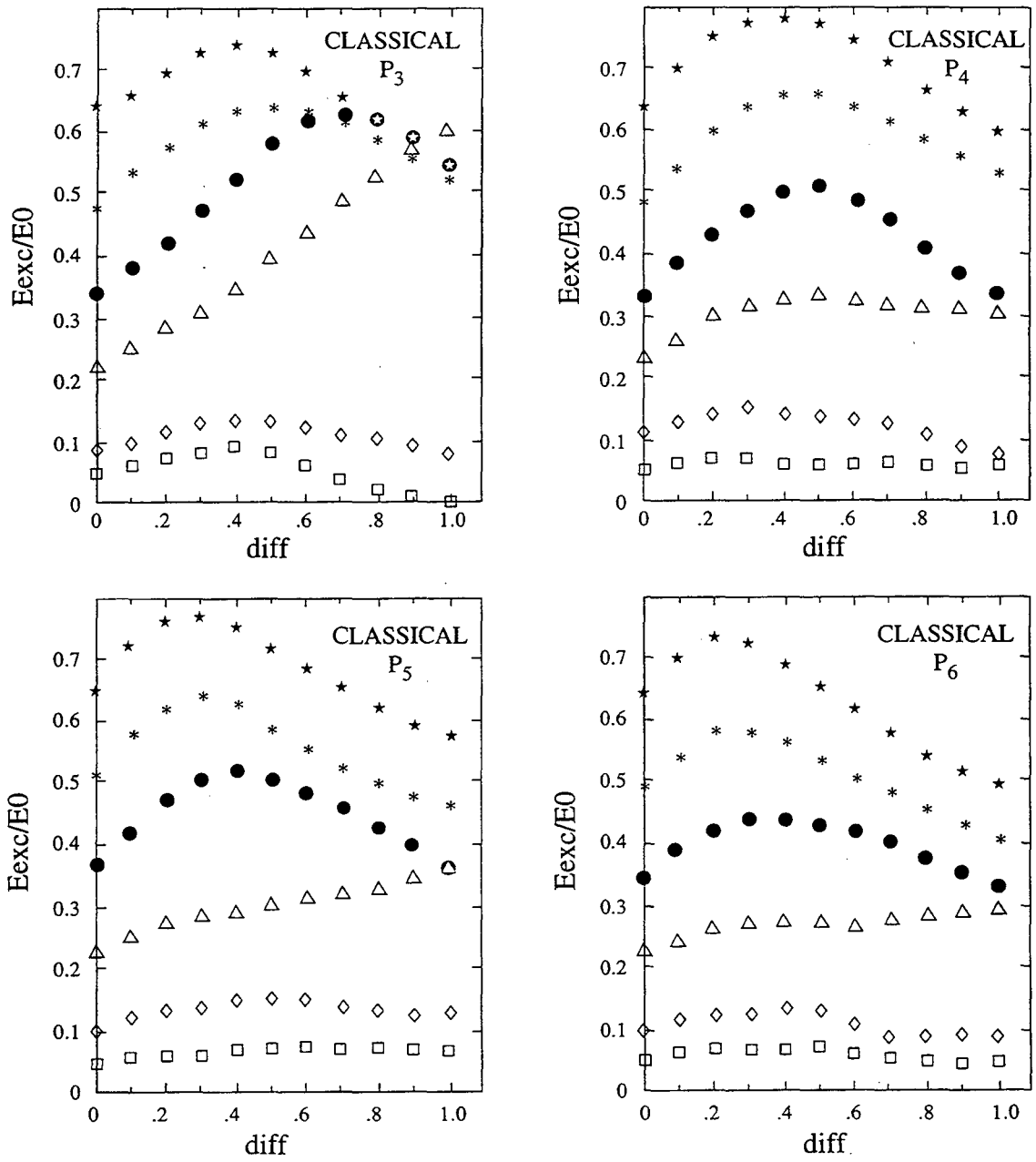
CLASSICAL
P3
CLASSICAL
P4
CLASSICAL
P5
CLASSICAL
P6
Eexc/E0
diff
0
0.1
0.2
0.3
0.4
0.5
0.6
0.7
.2
.4
.6
.8
1.0

$$R(\theta) \approx R_o\,(1 + 0.2683\,P_4)$$

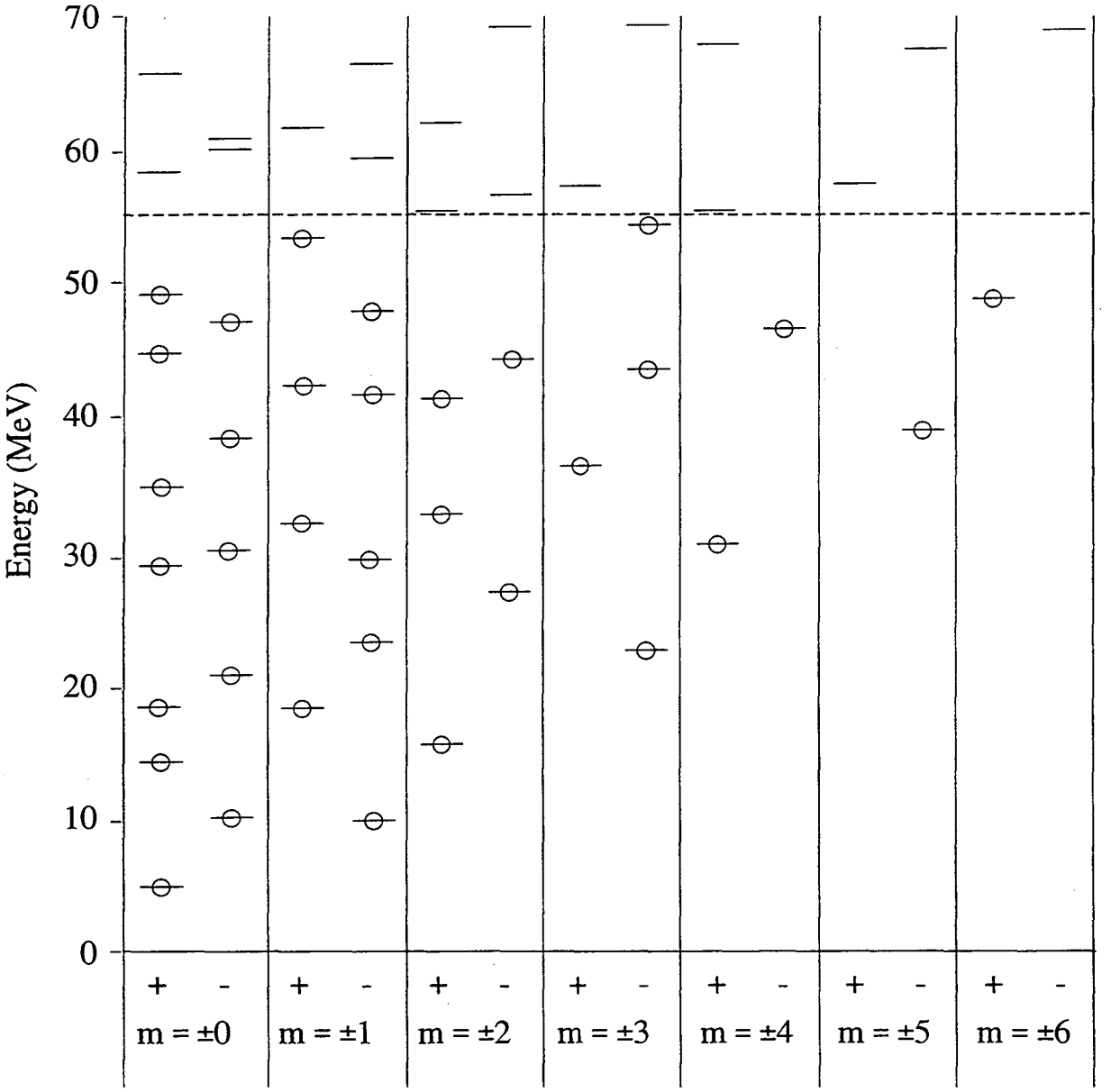

LAWRENCE BERKELEY LABORATORY
UNIVERSITY OF CALIFORNIA
TECHNICAL AND ELECTRONIC
INFORMATION DEPARTMENT
BERKELEY, CALIFORNIA 94720